

Structural origin of resistance drift in amorphous GeTe

Federico Zipoli,^{*} Daniel Krebs, and Alessandro Curioni*IBM Research – Zurich, Säumerstrasse 4, CH-8803 Rüschlikon, Switzerland*

(Received 20 November 2015; revised manuscript received 16 February 2016; published 11 March 2016)

We used atomistic simulations to study the origin of the change of resistance over time in the amorphous phase of GeTe, a prototypical phase-change material (PCM). Understanding the cause of resistance drift is one of the biggest challenges to improve multilevel storage technology. For this purpose, we generated amorphous structures via classical molecular-dynamics simulations under conditions as close as possible to the experimental operating ones of such memory devices. Moreover, we used the replica-exchange technique to generate structures comparable with those obtained in the experiment after long annealing that show an increase of resistance. This framework allowed us to overcome the main limitation of previous simulations, based on density-functional theory, that suffered from being computationally too expensive therefore limited to the nanosecond time scale. We found that resistance drift is caused by consumption of Ge atom clusters in which the coordination of at least one Ge atom differs from that of the crystalline phase and by removal of stretched bonds in the amorphous network, leading to a shift of the Fermi level towards the middle of the band gap. These results show that one route to design better memory devices based on current chalcogenide alloys is to reduce the resistance drift by increasing the rigidity of the amorphous network.

DOI: [10.1103/PhysRevB.93.115201](https://doi.org/10.1103/PhysRevB.93.115201)

I. INTRODUCTION

Phase-change materials (PCM) based on chalcogenide alloys are considered very promising for memory storage applications [1,2]. These alloys usually consist of Ge, Sb, and Te atoms. These materials are interesting because they undergo reversible and fast transitions between the amorphous and crystalline phases upon heating. The two phases have different electrical resistivity and optical properties, and these differences can be exploited to store and read the information [3,4].

To make phase-change memories competitive to flash, it is necessary to increase the storage density, for example, by storing multiple bits per cell, which means by being able to program more than two values of resistance in a single cell. The maximum number of states that can be written and read out at a later point in time is limited by the fact that the resistance of the amorphous phase increases over time, eventually leading to an overlap of the resistance levels [5,6].

Low-field electrical transport in amorphous phase-change materials can be described by trap-limited band transport at room temperature [7]. In this transport model, previous studies have attributed the increase of resistance to an increase of the activation energy of conduction [8–11]. Furthermore, by combining several spectroscopic measurements it could be shown that the density of states of GeTe is made up of tail states and defects in the band gap pinning the Fermi level [12]. Thus, an increase in activation energy could come from changes in the distributions of defects and tail states, causing the Fermi level to move, or from a shift of the valence band edge that increases the optical band gap.

In this work, we aim to address this topic and identify the structural changes responsible for the increase of activation energy for conduction. Therefore, our first aim is to link the density of states to the structures; in particular, we want to find which structural features are responsible for localized states in the band gap of amorphous GeTe (a-GeTe).

To produce sufficient statistics, we generated an ensemble of uncorrelated a-GeTe configurations via quenching from the melt of GeTe on a nanosecond time scale to match the operating conditions of the memory device [13]. Since it has been shown that the quenching rate critically determines in which state the glassy state is frozen [14–18], it is crucial to be as close as possible to the experimental time scales. First-principles (FP) calculations based on density-functional theory (DFT) have been widely used to study PCM materials [19–31]. DFT-based calculations provide an accurate tool to model both the structural and electronic properties of these systems. The main limitation of DFT, however, is that it is computationally demanding. Only relatively short time scales, compared to the experimental ones, limited to less than one nanosecond can be simulated for the typical systems consisting of a few hundreds of atoms. For this reason, we think that a deeper understanding of the mechanism responsible for the drift in PCM requires the use of classical molecular-dynamics (MD) simulations, which can model the system sizes and time scales mentioned above. We recently developed a classical augmented Tersoff-based short-range order reactive potential for GeTe [32], which was successfully validated against both experimental data and the DFT calculations by Sosso and coworkers [33], who, driven by the same reason, developed a classical neural-network-based potential.

Using classical MD to generate the structures and DFT with the help of hybrid functional [34] for the analysis, we found that most of electronic states in the gap are caused by groups of Ge atoms in which the coordination of at least one Ge atom differs from that of the crystalline phase. We anticipated part of these results in the proceedings of the EPCOS conference [35] which were independently confirmed by Raty *et al.* [36] and Gabardi *et al.* [37]. Besides showing a complete statistic of structures responsible for localized states in the band gap of a-GeTe, the second aim of this work is to address the question of which structural changes will occur upon relaxation over time and ultimately lead to an increase in resistance and compute when possible the activation energy barriers. For

^{*}Corresponding author: fzi@zurich.ibm.com

this purpose even traditional classical molecular-dynamics simulations are not sufficient, because breaking of bonds is an activated process involving an energy barrier that is too large compared to the thermal energy and does not occur within the typical duration of an MD simulation. In order to enhance the sampling of the configurational space, allowing breaking of covalent bonds, we made use of replica-exchange (RE) MD simulations [38,39] (cf. Methods, Sec. II B). The RE scheme cannot be easily coupled with DFT calculations because it requires running tens of replica in parallel for long time scales; see Methods, Sec. II. Thanks to our computational efficient classical potential, we were able to use for the first time the RE technique to explore more efficiently the energy landscape of a-GeTe producing more relaxed structures. This was the main motivation behind the use of an efficient classical potential towards DFT. The same approach proved to be successful for studying the role of defects in an a-Si network [40]. We found that an increase in resistance is correlated with a change in the topology of the bond network reducing the number of unoccupied states in the band gap leading to a shift of the Fermi level towards the middle of the band gap. Our results show that this reduction of localized states in amorphous GeTe is accompanied by a slow evolution of the bond network towards structures having a first-neighbor topology more similar to that of the crystalline phase. To support our model, we used first-principles Car-Parrinello molecular-dynamics simulations with the metadynamics technique [41,42] to study the evolution of a prototypical structure responsible for an empty state localized in the band gap into a lower energy configuration which results in a structure without gap states. We computed the minimum energy pathway at zero kelvin, which was optimized from the trajectory obtained via the metadynamics technique to get information on the barriers associated with the relaxation.

The paper is organized as follows: A brief description of the methods used to generate and analyze the structures is described in Sec. II. Our classical potential was validated in Ref. [32] against DFT results of previous works [23,33]. Results are illustrated in Sec. III and discussed in Sec. IV. Conclusions are given in Sec. V.

II. METHODS

This section illustrates the methods used to generate and analyze the amorphous structures.

A. Quenching via classical MD Simulations

We used classical MD simulations to generate structures by quenching on the nanosecond time scale. The interactions between Ge and Te atoms were modeled via a Tersoff-based potential of the type recently proposed [32]. For this work, we used the TERSMD code owned by IBM. For completeness we report that driven by the same idea, Sosso and coworkers developed a classical potential based on a neural network (NN) approach [33], which was successfully validated against the DFT calculations. We used the DFT results of Ref. [33] to benchmark our potential as extensively described in Ref. [32]. Molecular-dynamics simulations were carried out at constant temperature and volume, NVT ensemble. The results presented

in this work corresponds to the NVT simulations at density of 5.65 g/cm^3 , which is close to the experimental values of a-GeTe: $5.6 \pm 0.6 \text{ g/cm}^3$ and 5.7 g/cm^3 from Refs. [43,44], respectively. For computational efficiency, since we make use also of hybrid functionals, and to obtain enough statistics, we generated and analyzed 70 structures containing 216 atoms or 108 GeTe units. The choice of this box size was motivated by the fact that the bottleneck of the present study is the time required to refine the geometry optimization via DFT. This size allowed us to analyze the largest number of atoms per unit of time at the time the work started. We would like to point out that the relatively small box used in this work compared to the most recent calculations carried out by Sosso *et al.* [45] and Gabardi *et al.* [37] poses a limit on the size of the defects than can form. Despite this limitation, we were still able to identify the key structural changes responsible for resistance drift.

To generate a-GeTe structures, we used two different protocols: quenching from the melt via MD simulations and annealing via replica exchange [38,39] MD simulations as described in Methods, Sec. II B. In both approaches, the temperature was maintained constant via a Berendsen thermostat [46] with a coupling parameter of 2.4 ps. This parameter determines how tightly the bath and the system are coupled together. Because of the large mass of the atoms, we used a time step of 2.4 fs to integrate the equation of motion.

We melted the system by heating the 108 GeTe units up to 1000 K in a $18.521\text{-}\text{\AA}$ large cubic box. Then, we reduced the temperature in discrete steps of 10 K from 985 to 300 K with each simulation lasting a total of 4 ns. A time of 4 ns corresponds to the experimental conditions typically used to program phase-change memory cells into the high-resistive amorphous RESET state [13].

B. Annealing via replica-exchange MD simulations

To generate structures with varying states of structural relaxation, we annealed a initial structure taken from a simulation at $T = 1000 \text{ K}$ via replica-exchange [38,39] MD simulations. This technique allows one to explore the phase space efficiently allowing structures to overcome barriers in the energy landscape. We used 256 replicas with the same number of atoms and box size as in the quenching via MD. The temperatures of the replicas, ranging from 300 to 1500 K, were exponentially spaced. Replicas were exchanged according to the Metropolis algorithm every 12 ps [47]. Hundreds of replica-exchange steps were performed to explore the phase space, resulting in a total annealing time on the nanosecond time scale. At temperatures lower than 470 K, we found the formation of crystalline GeTe, which is the stable phase. At temperatures higher than 470 K, we observed loss of long-range order. We selected these structures resulting from temperatures above 470 K as representative of a-GeTe structures.

C. Modified classical potential

To look for structures that potentially feature fewer defect states, we generated an additional 21 a-GeTe structures by modifying the classical potential to increase the sampling of structures that would not be easily produced otherwise because

crystallization will occur. The motivation for this additional set of calculations is related to the outcome of the DFT analysis, which showed that most of the electronic states localized in the band gap we produced by groups of Ge atoms with specific characteristics.

The modification of the potential consisted in the removal of the attractive part of the interaction between Ge-Ge and Te-Te pairs by setting the parameter B_{IJ} of the Morse potential to zero (see Table 1 in Ref. [32]), while keeping the cross terms of the Ge-Te pairs unchanged. The effect of this modification is to bias the systems towards structures with fewer Ge-Ge pairs. Our aim was to see whether these structures, produced by the modified potential, had fewer electron states localized in the band gap. Three of the 21 structures were quenched using the protocol as explained in Sec. II A. The other 18 structures were quenched and annealed via RE-MD (cf. Sec. II B).

D. Computational details of first-principles calculations

First-principles calculations based on DFT were used to optimize the structures obtained via classical simulations and to characterize the electronic properties.

The FP simulations were performed within the framework of DFT in the local density approximation supplemented by generalized-gradient corrections [48], as implemented in the CPMD code [49]. This functional has been successfully used in previous works without van der Waals (vdW) correction [23,37,50]. Comparison between DFT and EXAFS experiments [51] shows that PBE tends to overestimate the bond lengths; see first peak of the pair correlation function in the supplemental material of Ref. [23]. We did not include empirical van der Waals correction, which have been shown to be more important in other alloys containing less germanium than tellurium [52], such as $\text{Ge}_{15}\text{Te}_{85}$ and $\text{Ge}_2\text{Sb}_2\text{Te}_5$. We used Goedecker-Teter-Hutter pseudopotentials [53] with a plane-wave expansion of the Kohn-Sham orbitals up to a kinetic energy cutoff of 80 Ry. We used only the Γ point to sample the Brillouin zone (BZ). For geometry optimizations and energy-barrier determination, the norm of the force vector was required to be smaller than $5 \text{ meV}/\text{\AA}$ at convergence. Such a tight convergence criterion is necessary for phase-change material systems with floppy vibrational modes [54]. The properties involving virtual states were computed using the hybrid functional HSE [34]; see Sec. II F to better reproduce the band gap [50].

E. Bond network characterization

Structures obtained via MD and optimized via DFT were analyzed via the Wannier-functions (WF) scheme [55,56]. This procedure provides a powerful tool for an unambiguous characterization of the bond network. In the supplemental information of Ref. [32], we already introduced the WF-based analysis for GeTe. The idea is that we use the center of charge of the WF, known as the Wannier center (WC), to establish whether two atoms are connected by a bond or not (see Fig. 1). Wannier centers can be used to identify the presence lone pairs [55,57]. In the crystalline and amorphous phase of GeTe we never observed spin polarization, which indicates the absence of radicals and dangling bonds. When a bond is

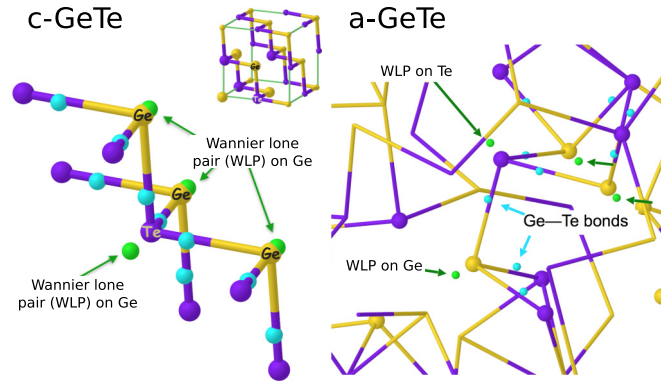


FIG. 1. Bond network in crystalline (c-GeTe) and amorphous (a-GeTe) germanium-telluride. Wannier centers corresponding to bonds are depicted by light blue spheres. Wannier lone pairs (WLP) are depicted by green spheres. For clarity only a small number of WC is illustrated. For completeness, we report that the spread values of the Wannier functions (WF) for c-GeTe are 3.06, 3.18, and 3.20 a.u. for WF corresponding to lone pairs on Ge, lone pairs on Te, and bonds, respectively.

present between two atoms, the relative position of the WC along the bond is a direct measure of the polarization [57]. For heterobonding, in general, the WC is closer to the tellurium atom, which is more electronegative than the Ge atom; but exceptions may occur in defective configurations, e.g., when atoms have higher/lower coordination.

F. Calculation of optical conductivity

To sort the large number of systems, an order parameter is necessary that can correlate structural changes to the experimentally observed change in resistance in the material. The optical conductivity is a natural choice for such an order parameter.

Kohn-Sham (KS) states were computed with both PBE [48] and the hybrid functional HSE [34]; the latter functional, HSE, has been demonstrated to correct the band gap for these phase-change materials [22]. We analyzed the KS orbitals whose eigenvalues were within an interval of $-0.1, 0.5 \text{ eV}$ around the Fermi energy. About 70 % of these states could easily be related to the four types of structures shown in Fig. 2.

Using both the PBE and HSE functionals, we computed the optical conductivity $\sigma(E)$ as a function of the excitation energy E defined by

$$\sigma(E) = \frac{2\pi\hbar e^2}{3m_e^2 V_{\text{cell}}} \frac{1}{E} \sum_{i,j} (f_i - f_j) |\langle \psi_j | \hat{p} | \psi_i \rangle|^2 \delta(\varepsilon_j - \varepsilon_i - E), \quad (1)$$

where e is the elementary charge, m_e is the electron mass, p is the momentum operator, V_{cell} is the volume of the box, \hat{p} is the momentum operator, ψ_i are the KS orbitals, ε_i are their corresponding eigenvalues, and f_i are their occupation numbers. To assign a conductivity to each structure, we averaged the optical conductivity from zero to an arbitrarily selected value $E_{\text{cut}} = 0.98 \text{ eV}$ as follows:

$$\bar{\sigma} = \frac{1}{E_{\text{cut}}} \int_0^{E_{\text{cut}}} \sigma(E) dE. \quad (2)$$

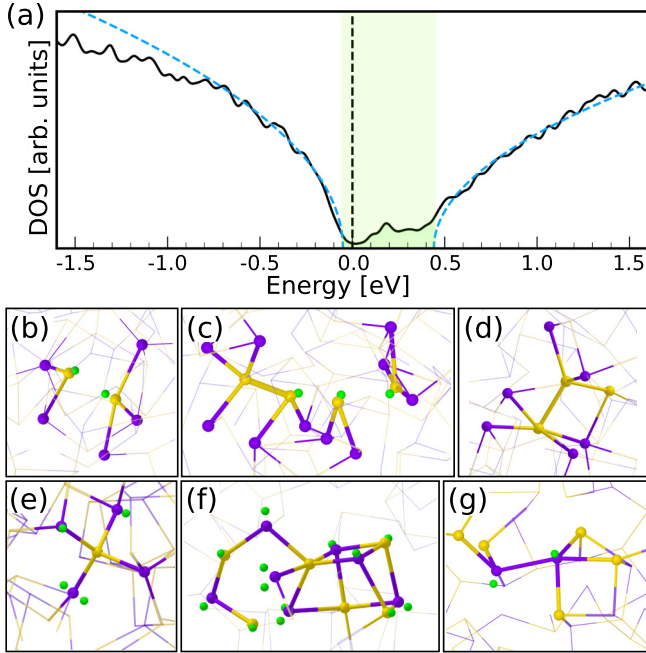


FIG. 2. (a) Electronic density of states (DOS) computed within DFT using the HSE functional (solid black line). KS eigenvalues were smeared with Gaussians of 25 -meV width. The zero in the x axis corresponds to the Fermi energy computed at $T = 300$ K (dotted black line). A parabolic fit of the DOS is plotted for comparison (dashed light blue lines). The energy range corresponding to the band gap is colored in light green. (b)–(g) Examples of structures producing localized states in the band gap. Ge and Te atoms are depicted as dark yellow and violet spheres, respectively. Bonds between these atoms are depicted by cylinders. The bond network of the surrounding atoms is indicated by thin lines. Wannier lone pairs (WLP) close to the defects are depicted by green spheres. (b)–(d) Examples of the statistically most relevant defect with clusters of Ge atoms, non-necessarily bonded, close to each other in which at least one Ge atom is over- or under-coordinated. (e) Fourfold coordinated Ge atom in tetrahedral configuration. (f) GeTe cubes not properly aligned sharing a Ge atom. (g) A pair of Te atoms connected by a bond in which one of the two atoms is over-coordinated.

This order parameter $\bar{\sigma}$ was used to sort the large number of simulated structures.

G. Car-Parrinello MD simulations

To simulate the evolution of a structure associated with a groups of Ge atoms that produced a localized state in the band gap, we used first-principles Car-Parrinello MD (CPMD) simulations combined with the metadynamics technique [41,42], which allows large barriers to be overcome in affordable simulation time (few picoseconds) [41]. The metadynamics technique is based on a coarse-grained non-Markovian dynamics in the manifold spanned by few reaction coordinates, biased by a history-dependent potential that drives the system towards the lowest saddle point. The main assumption is that the reaction path could be described by a few collective coordinate functions of the ionic coordinates. Following the scheme of Ref. [42], the first-principles Lagrangian is supplemented by

a history-dependent external potential which acts on the ionic coordinates. The history-dependent potential is constructed by the accumulation of Gaussians, centered at the positions of the states already visited along the trajectory. This potential discourages the system from remaining in the regions already visited and pushes it over the lowest energy barrier towards a new equilibrium basin. This technique was used only to find the reactive pathways, because longer simulations are required to accurately estimate the free-energy barriers along such a complex energy landscape. In the metadynamics scheme, we have to choose some collective variables suitable to describe the reaction and discriminate the reagents and products. The result may depend on the particular set of collective variables used. In this work we did not carry out extensive simulations to compare different choices. Our goal was, first, to find out if removal of this particular defect resulted in a lower energy structure without the KS state in the band gap and, second, to compute the energy of the process along the reactive pathway found. The activation energy barrier computed with this approach is an upper bound, because we cannot exclude that there are other pathways with lower activation energies. Details on the CPMD simulations and on the choice of the reaction coordinated for the metadynamics simulation are given in the Supplemental Material [58]. We used the nudged-elastic band method (NEB) [59] to compute the energy barriers along the reactive path guessed via the metadynamics. Because there are many local minima, the path connecting the initial and final configurations was split into 10 parts.

III. RESULTS

We generated two sets of amorphous structures using two different methods: quenching from the melt via MD simulations and RE MD simulations, respectively. Amorphous GeTe structures produced via quenching should correspond to the experimental amorphous phase obtained immediately after the fast cooling, whereas replica-exchange MD should produce more stable a-GeTe structures comparable to those obtained in the experiment after annealing at temperatures of about 350–400 K that show an increase of resistance. Using our Tersoff-based potential, we created 17 a-GeTe structures containing 216 atoms by quenching from the liquid at 985 K in 4 ns to 300 K via classical MD, to be as close to experimental conditions as possible (cf. Methods, Sec. II A). FP DFT calculations were used to characterize the electronic properties of these structures. In order to enhance the sampling, we created an additional set of 27 a-GeTe structures containing 216 atoms via RE MD simulations. 300 K via classical MD, to be as close to experimental conditions as possible (cf. methods section II A). FP DFT calculation were used to characterize the electronic properties of these structures. In order to enhance the sampling, we created an additional set of 27 a-GeTe structures containing 216 atoms via RE MD simulations.

A. Structures producing electronic states in the band gap of a-GeTe

In this section, we aim to answer the question: *What kind of structures are producing states in the band gap of amorphous GeTe?* In a crystal, one “good” bond configuration dominates

the structure, resulting in a well-defined electronic band structure. Deviations from this preferred bond configuration are called defects and may produce states in the band gap. Amorphous systems, however, typically exhibit a structure that is built up by local bond configurations, which form small units that are randomly connected to each other; thus a structure with a large variety of configurations in coordination, bond distance, bond angles, etc., results [60]. In amorphous systems, such as phase-change materials [61–63], in order to determine defects, one has to assess whether there is one energetically most favorable local topology that makes up the bands. Deviations from this “ideal” local order that gives rise to band tails and gap states may be defined as defect. We analyzed 44 structures, each containing 216 atoms, which were generated using a classical potential for GeTe of the type developed in Ref. [32] via quenching (cf. Sec. II A) and via replica-exchange (cf. Sec. II B). The large number of structures allows us to perform statistical analysis to find correlation between structural features and the density of states (DOS).

Figure 2(a) shows the averaged electronic density of states (DOS) of the 44 structures computed using the hybrid HSE functional [34] (cf. Methods, Sec. II D). The average DOS can be described by a valence and conduction band with parabolic shape and a band gap of about 0.5 eV, slightly underestimating the experimental value. Furthermore, the gap is occupied by localized states pushing the Fermi level towards the valence band, which confirms the predominant hole contribution to transport [7].

Because of the large number of configurations in our study, we were able to extract the statistics of configurations responsible for localized states in the band gap, namely, from -0.05 eV to 0.45 eV in Fig. 2(a). Figures 2(b)–2(g) illustrate those defect states in the gap. About 55 % of the defect states are produced by groups of Ge atoms which are not necessarily covalently bonded but closer than 2.8 Å and in which the coordination of at least one Ge atom differs from that of the crystalline phase: three bonds and one lone pair; see Figs. 2(b)–2(d). We also identified the other three types of defects present in lower concentrations, of about 5 % each. Those are fourfold tetrahedral coordinated Ge atoms [see Fig. 2(e)], close cubes not properly aligned [see Fig. 2(f)], and pairs of Te atoms at distances shorter than 4 Å [see Fig. 2(g)], and most of the times associated with close cubes not properly aligned. For all those cases in which a state is associated with more than one of the four categories listed above, we assigned that state to both categories, with weight equal to one-half, to construct the statistic.

B. Topology of the bond network in a-GeTe

In this work, the topology of the amorphous network is always determined using localized Wannier functions (WF) [55] (see Sec. II E). This approach proved to be very useful in analyzing disordered systems [56]. Details are given in the supplemental information of Ref. [32]. We already pointed out [32,35] the importance of a DFT-based approach to establish the presence of a bond between a pair of atoms versus the commonly used distance criteria, which we found not adequate to describe the bond network of GeTe. Via this analysis we showed in our previous report the presence of lone pairs in

a-GeTe and which configurations are responsible for electron states localized in the band gap [35]. Thereafter, these results were confirmed by other DFT-based approaches characterizing bonds based on charge density difference [64,65] and more recently based on the crystal orbital overlap population [66]. These works [64,66] show that a simple distance criteria is not sufficient to characterize the bond network.

In the previous section, we used the coordination of crystalline GeTe as a reference to define over- and under-coordinated atoms. In the crystalline phase, both Ge and Te atoms are threefold coordinated, with a lone pair being localized on each of them. We refer to this type of configuration as Ge[3+1] or Te[3+1], respectively, where the number before and after the “+” indicates the number of bonds and Wannier lone pairs. However, the terms of over- or under-coordination should rather refer to the preferred nondefective structure in amorphous GeTe. To investigate this preferred topology that the system evolves to, we need to sort our data using a meaningful order parameter. Empirically it is known that the electrical conductivity in phase-change materials decreases when the system relaxes over time. Thus, the averaged optical conductivity $\bar{\sigma}$ as defined in Sec. II F is a natural choice to determine which structures are more relaxed and thus show a preferred topology.

We grouped the 44 structures generated via quenching and replica exchange into five groups ranging from 1 (higher conductivity) to 5 (lower conductivity) and containing 14, 10, 14, 4, and 2 structures, respectively. $\bar{\sigma}$ spans values from just below 500 S/cm to 3000 S/cm. Each group covers an interval of 500 S/cm. The average topology of Ge-Te bonds of each of these five groups was analyzed using the Wannier-functions scheme described in Methods, Sec. II E. For various structural properties, such as the coordination number, number of Wannier lone pairs, bond distance and angles, bond polarization, etc., we found a significant correlation between the distribution of bond distances and polarizations of the network and the value of $\bar{\sigma}$. The result of this analysis is shown in Fig. 3. The histograms of normalized bond polarizations and bond distances for each group shows that upon relaxation, the topology of a-GeTe tends towards Ge-Te bonds, with a distance of approximately 2.8 Å and a bond polarization of 0.35, resembling the local order of the crystal. Thus, those configurations are called “good bonds,” and all other configurations can be regarded as deviation from the ideal topology. In particular, the Ge-Te bonds with the center of charge closer to the Ge atoms correspond to defective structures with over/under-coordinated atoms. To link changes of the bond network to the density of states, we calculated the DOS averaged over the configurations of each group [see Fig. 3(f)]. While the band gap remains rather constant, we observe a lowering of the number of states in the band gap moving from group 1 (GR.1) to group 5 (GR.5). The bleaching of these band-gap states, which are mostly unoccupied, leads to a shift of the Fermi level towards the middle of the band gap.

C. Resistance drift and the “ideal” a-GeTe

Based on the insights about the preferred topology and defective bond configurations, we next looked further into the

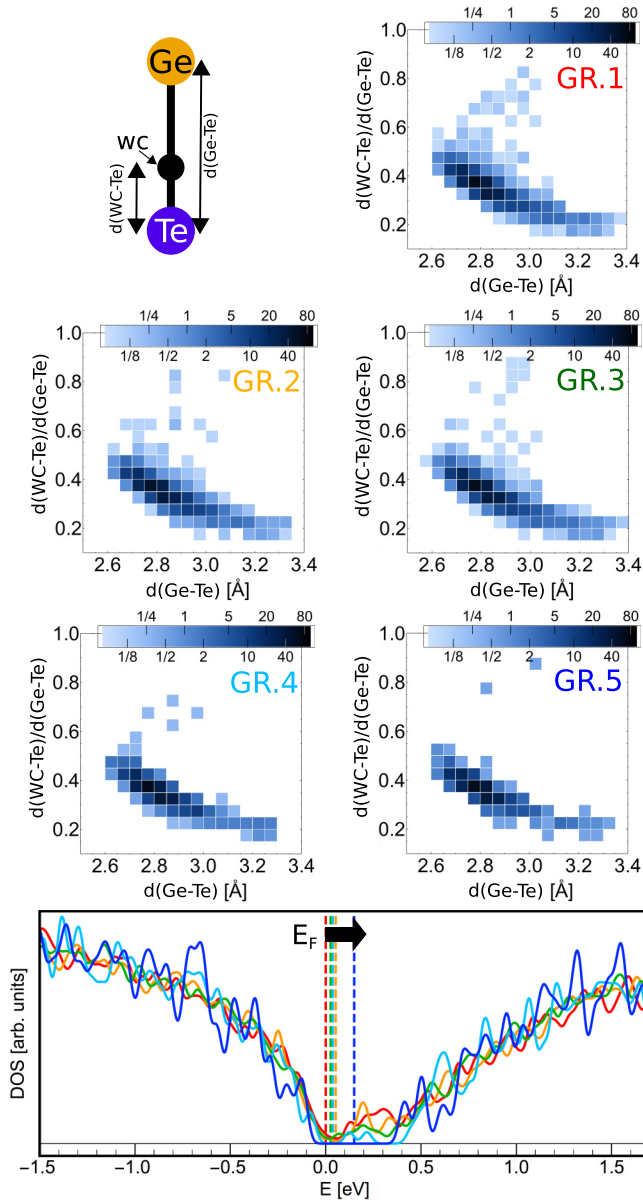


FIG. 3. Histograms of the position of the center of charge of the Ge-Te bonds (WC) versus the Ge-Te bond distance of the structures obtained via MD and RE-MD. The structures are divided into five groups sorted by decreasing averaged optical conductivity $\bar{\sigma}$. The corresponding histograms are shown. The y axis is the distance between the WC and the Te atom normalized by the Ge-Te bond length, a direct measure of the polarization of the bonds. The Ge-Te bond length is plotted on the x axis. The color scale indicates the number of bonds in each bin. Configurations with lower conductivity show a less sparse distribution. The last panel shows the average DOS of each of the five groups (red, orange, green, light and dark blue from group 1 to group 5). The decrease of $\bar{\sigma}$ is accompanied by a decrease in defect density, causing the Fermi level to shift towards mid-gap. The DOS was computed using the HSE functional, and the KS eigenvalues were smeared with Gaussians of 25 -meV width. A similar plot containing all the structures produced in this work, including those with the modified potential and resulting from the annealing, is given in Fig. 7.

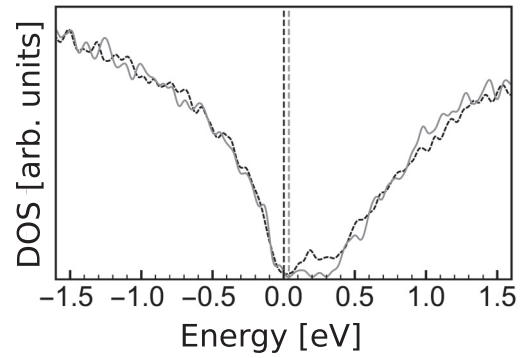


FIG. 4. Electronic density of states (DOS) computed within DFT using the HSE functional using the standard potential (dashed black line) and its modified version (solid gray line). The Fermi energy levels computed at $T = 300$ K for the two DOSs are indicated as vertical dashed lines in the corresponding color. While the band gap is rather similar in both cases, the number of gap states is significantly reduced by the modified potential, which favors Ge-Te “good” bonds. The DOS is constructed by smearing the KS eigenvalues with Gaussians of 25 -meV width.

two questions: *What is the ideal GeTe glass? What changes structurally upon relaxation towards the ideal amorphous GeTe?* Driven by our finding that about 55 % of the states localized in the band gap can be reconnected to groups of Ge atoms close to each other with an over- and under-coordinated Ge atom, we investigated the role of these Ge atoms in more detail by producing additional a-GeTe structures by modifying the classical potential (cf. Methods, Sec. IIC). The modification consists in the removal of the attractive part of the interaction between Ge-Ge and Te-Te pairs. This will bias the systems towards structures having fewer Ge atoms close to each other one thus having more Ge-Te pairs. Modification of the potential is a practical way to increase the sampling of configurations that would not be easy to produce otherwise, because, owing to the relatively small simulation size, the entropic barrier for crystallization is reduced, which results in a higher probability of crystallization than in the experiments.

In Fig. 4, the average DOS of the simulations with the original, classical potential [as shown in Fig. 2(a)] is compared with the average DOS of the 21 structures obtained using the modified potential. Indeed, the configurations obtained by suppressing the formation of Ge-Ge and Te-Te bonds have a lower DOS localized in the band gap. We still notice defects associated with the clustering of Ge atoms with the characteristics described above [see Figs. 2(b)–2(d)], but on average they are present at lower concentrations. Consequently, the Fermi level moves towards mid-gap, increasing the activation energy for conduction and thus resulting in an increased resistance.

Analogous to the procedure applied before for the structures created using the original potential, we can now look for trends in bond configurations in this extended data set including the structures from the modified potential, which are representative of more relaxed structures. Thus, when sorting all 65 obtained structures by the averaged optical conductivity as order parameter, any entity correlated to drift should have a significant trend.

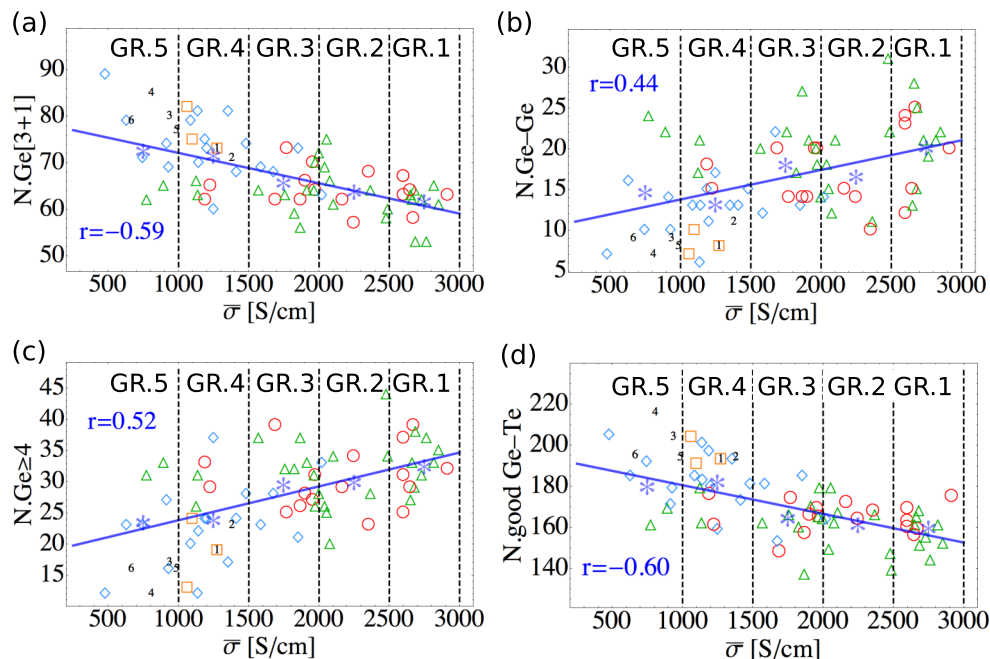


FIG. 5. Structural features as a function of the averaged optical conductivity $\bar{\sigma}$ for all a-GeTe structures generated in this work. The structural features more correlated with changes in optical conductivity are the number of (a) threefold coordinated Ge atoms with one lone pair (Ge[3+1]), (b) Ge-Ge bonds, (c) Ge atoms with coordination greater than three, and (d) “good” Ge-Te bonds (see also Table I). Different symbols are used to distinguish the method used to generate the structures: MD and RE-MD with the standard potential are indicated as red circles and green triangles, respectively. MD and RE-MD with modified potential are shown as orange squares and blue diamonds, respectively. Numbers from 2–6 indicate the structures obtained via first-principles Car-Parrinello MD (CPMD) simulations starting from structure 1. The blue line is the correlation of the data, which is given by r in each panel. The vertical panels separated by dotted gray lines indicate the groups.

We looked at various features in the structures, such as the coordination numbers, bond angles and polarization, number of Ge-Ge, Te-Te, and Ge-Te bonds, number of Wannier lone pairs, and number of four-membered rings and cubes, using the Wannier analysis described in Sec. II E. With the scheme proposed by Akola and coworkers [19], we also searched for vacancies which have been shown to be present in a-GeTe and in the amorphous phase of Ge₂Sb₂Te₅ (GST) [19,26]. We identified the structural configurations that show the most significant change with order parameter. Those trends are shown in Fig. 5. The unstrained Ge-Te bonds with a bond length between 2.725–2.825 Å and the center of charge located at 30%–40% closer to the Te atom along the Ge-Te bond are called “good” Ge-Te bonds in this work. A similar definition was proposed in our previous work [35]. The analysis shows that an increase of conductivity is strongly correlated with a reduction of the number of threefold coordinated Ge atoms with one lone pair, a reduction of Ge-Ge bonds, and of Ge atoms with coordination greater than three.

To extract the statistics of these trends, we divided the 65 structures into five new groups of decreasing value of $\bar{\sigma}$ with the same criteria used for Fig. 3, but now including also the 21 configurations obtained with the modified potential. The average numbers of relevant configurations of each group are summarized in Table I. Based on these results, we conclude that the questions raised in the beginning of this section can be answered in the following way: We propose that, over time, a change in resistivity is produced by both an ordering of the bond network by removal of stretched bonds

and by consumption “defects,” mostly Ge-Ge bonds and over-coordinated Ge atoms formed during the fast quenching, while increasing the number of Ge[3+1]. Our model shows that the reduction of these defects results from an evolution of the bond network towards structures having a first-neighbor topology more similar to that of the crystalline phase.

D. Relaxation process in a-GeTe

After addressing the questions of which kind of topology and defects the unrelaxed amorphous structure exhibits and to which ideal structure it relaxes, it remains to answer the

TABLE I. Average topology of five groups of independently generated structures ordered by decreasing averaged optical conductivity $\bar{\sigma}$. The entries in the table are the number of structures in each group (No. str.), the number of threefold coordinated Ge atoms with one lone pair (Ge[3+1]), the number of Ge-Ge bonds (Ge-Ge), the number of Ge atoms with coordination greater than three ($\text{Ge} \geq 4$), and number of “good” Ge-Te bonds, that have a bond length between 2.725–2.825 Å and a center of charge located at 30%–40% closer to the Te atom along the Ge-Te bond.

	No. str.	Ge[3+1]	Ge-Ge	$\text{Ge} \geq 4$	“Good” Ge-Te
GR. 1	14	61.8	20.2	32.6	159.9
GR. 2	11	63.9	16.6	30.0	161.5
GR. 3	17	65.8	18.1	29.6	164.8
GR. 4	16	71.7	13.2	23.9	182.4
GR. 5	7	72.7	14.7	23.6	180.3

following question: *How does the relaxation occur?* In the 1980s, Gibbs *et al.* [67] proposed a description for relaxation kinetics in amorphous materials that today is probably the most widely used model in various classes of materials. However, for systems in which relaxation towards equilibrium evolves logarithmically over many orders of magnitude in time, Gibbs' model requires a very specific distribution of activation energies for relaxation. For polymers, Knoll *et al.* [68] showed that an alternative description originally proposed by Egami [69] for metallic glasses can describe the relaxation process on the basis of a single activation energy that increases with time.

To shine a light on this controversy about the energy barriers involved and to show that, indeed, less defective structures are energetically more favorable in phase-change materials, we used CPMD simulations combined with the metadynamics technique (cf. Sec. II G) to explore the reaction mechanisms of a local structure associated with a state localized in the band gap. We found that removal of this defect results in a new structure that is lower in energy [see Fig. 6(a)]. The DOS of the local minima indicated by colored numbers is plotted in Fig. 6(c) and shows how eventually the band gap is cleaned from defects. We computed the minimum energy path (MEP) at zero temperature using nudged-elastic band (NEB) calculations. The MEP, plotted in Fig. 6(b), shows that the largest activation energy barriers involved in this structural relaxation are about 1 eV. The length of the reactive path, which is computed by summation of the displacements of all the atoms along the MEP, is about 40 Å and indicates the extent of relaxation of the defect and its environment. Although we computed only the energy barrier for a single process, this single MEP has to be seen as a prototypical energy landscape for a structural relaxation in a-GeTe involving a series of local minima separated by a broad energy barrier spanning from the thermal energy to about 1 eV. Although the MEP is computed at zero temperature, we do not expect the entropic contribution to modify substantially the free-energy landscape along the reacting path.

IV. DISCUSSION

DOS evolution. Our results show that a preferred local order in the amorphous phase exists. Upon relaxation, the bond network rearranges such that this preferred local order is obtained everywhere in the structure, forming the ideal GeTe glass. As shown above, certain bond configurations that differ from the preferred local order in unrelaxed a-GeTe form defect states in the band gap. Consequently, upon relaxation, the density of those defects decreases while the structure evolves towards the ideal glass. This is illustrated in the DOS plot in Fig. 3(f) for the 44 structures generated using the classical potential. Another way of presenting the DOS evolution is by plotting the optical conductivity, $\sigma(E)$; cf. Methods, Sec. II F. Figure 7 shows the calculated DOS for the five groups from Table I, in Fig. 7(a) the calculated optical conductivity in Fig. 7(b), and for comparison experimental absorption data [10] in Fig. 7(c).

The experimental data were obtained on a thin film sample, which was annealed below the crystallization temperature between subsequent absorption measurements to accelerate

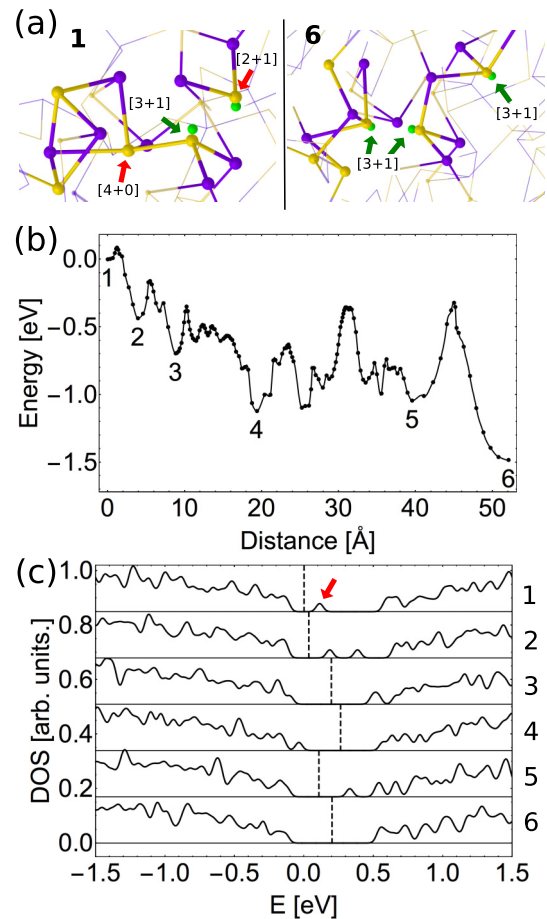


FIG. 6. (a) a-GeTe configurations before (left) and after (right) annealing via CPMD simulations. Ge and Te atoms are depicted as dark yellow and violet spheres, respectively. Wannier lone pairs close to the defects are depicted as green spheres. The red arrows in (a) indicate Ge atoms whose coordinations differ from [3+1], which stands for three bonds and a Wannier lone pair. In the initial configuration, the under-coordinated Ge atom [2+1] produces a defect in the band gap as shown in (c). As a result of the annealing, the three Ge atoms have coordination [3+1] and the defect in the gap has vanished; cf. 6 in (c). (b) Minimum energy path optimized via NEB calculations. The path connects the initial and the final structures, plotting the total distance that all atoms moved on the x axis. (c) Evolution of the DOS along the reaction pathways computed via DFT using the HSE functional. The vertical dashed lines indicate the Fermi energy at $T = 300$ K.

relaxation. Whereas previously the absorption data have been interpreted with an increase of the band gap, which indeed would lead to the observed shift of the absorption data, our calculation suggests a different interpretation (see Fig. 7): The decrease of the density of defect states as observed in our calculations results in a reduced optical conductivity at energies lower than the band gap for more relaxed structures. At high energies, the difference vanishes because the band gap stays constant in our calculations. In the experimental data, this trend is also visible even though not as pronounced as in our calculation.

Relaxation kinetics. In this work, we investigated the temporal evolution of a selected structure containing a structural

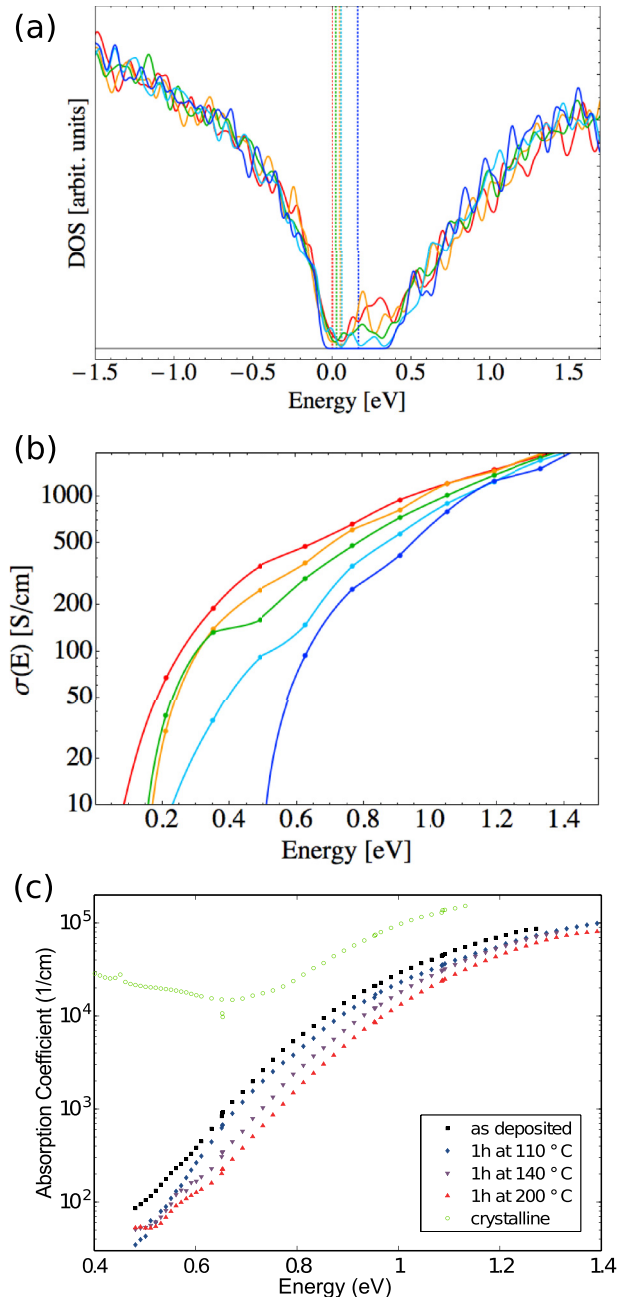


FIG. 7. Electron density of states of each of the five groups of Table I. The colors red, orange, green, light and dark blue in (a) and (b) label the different groups from 1 to 5, respectively. The HSE functional was used and the KS eigenvalues were smeared with Gaussians of 25 meV width. From group 1 to 5, we find a shift of the Fermi energy towards the middle of the band gap caused by consumption of states associated with defects in the band gap. (b) Calculated optical conductivity. The color code is the same as in (a). The DOS in (a) shows that the changes in optical conductivity are related to a decrease of states in the band gap rather than to an opening of the band gap. (c) Experimentally obtained absorption coefficient from Ref. [10]. Both the computed optical conductivity and the experimentally obtained absorption data shift towards higher energy. This suggests a correlation between drift, experimentally accelerated via annealing, and a decrease in gap states as observed via MD calculations, causing a shift of the optical conductivity to higher energies.

defect responsible for a single localized state in the band gap that is otherwise clean. We used CPMD simulations to anneal the defect and then we computed the activation energy barriers at the DFT PBE level at zero temperature. For this process to occur, we found a complex energy landscape characterized by multiple minima separated by activation energy barriers spanning from thermal energy to about 1 eV, which is the highest barrier height along the reaction pathway. This barrier determines the time scale of the relaxation event illustrated in Fig. 6. Even though our work provides a snapshot of the barriers involved in a single relaxation event, further work is necessary to provide statistics for many independent rearrangements to enable a kinetic description of the macroscopic relaxation process. In addition we would like to stress that further work should require the use of larger simulation boxes containing thousands of atoms to mitigate the size effects that are indeed present in our simulation cell less than 20 Å wide. As most recent calculations carried out by Sosso *et al.* [45] show that long Ge-Ge chains can form in GeTe systems.

We would like also to point out our definition of defect, which we proposed in Ref. [35] and used also in the current work, is relatively similar to that given in Ref. [37], in particular we can distinguish the following cases. Some of the defects we found consists of Ge-Ge bonds, exactly as reported in Ref. [37]. There are other cases, in which the same defect would be called a chain of Ge atoms connected by bonds according to Gabardi's definition and a group of Ge atoms that are not necessarily connected by bonds according to our definition based on Wannier functions. We identify the same structure with two different names because we consider a bond between two atoms only when there is a Wannier center associated with it. This is a more rigorous way to assign a bond compared to a distance criteria; see Methods. More in general we consider defects also all the clusters consisting of Ge atoms in which there is at least one Ge atom not forming three Ge-Te bonds or not having a lone pair, for example, one of the two Ge atoms forming the defect in Fig. 2(b) is twofold coordinated, therefore, this is a defect.

Valence alternation pairs. Frequently, valence alternation pairs are suggested to be the defects responsible for electrical transport and switching behavior in phase change materials. In the original works [62,70], they were proposed to explain the pinning of the Fermi level by deep defects in the absence of unpaired spins that otherwise would have been detected by electron spin resonance (ESR). The suggested valence alternation pair defects consist of one over-coordinated (threefold) and one under-coordinated (onelfold) chalcogen atom.

The main defects in GeTe are similar in nature, but not as simple as suggested in the valence alternation pair model. The "ideal" GeTe structure tends towards Ge and Te coordination with three bonds and one Wannier lone pair. The main defects that produce states in the gap are groups of Ge atoms, closer than 2.8 Å but not bonded to each other, in which at least one Ge atom is over- or under-coordinated. Thus, defects originate from unfavorable coordination with respect to the bonding in the crystalline phase. Those defects determine the position of the Fermi level and thus the p-type character of GeTe. All electrons in those defects are paired, either in

bonds or lone pairs, which explains the absence of an ESR signal.

Tetrahedral vs octahedral. While above we focused our discussion on those features with the highest correlation to a change in conductivity, we also want to comment briefly on the bond-angle distributions in our structures, to put into the context of previous works that point out the importance of tetrahedral and octahedral bond configurations for relaxation [71–74]. Takahashi *et al.* [72] concluded, from a comparison of their XPS/UPS data with calculations from O’Reilly *et al.* [71], that Ge-rich GeTe deposited at 77 K is mostly threefold coordinated with 99.9° bond angles, and it relaxes to a fourfold coordination with 109.5° bond angles, i.e., tetrahedral coordination. In contrast, XANES studies by Mitrofanov *et al.* indicate a conversion of tetrahedrally coordinated Ge sites into threefold coordinated octahedral sites upon relaxation [74]. Hosokawa *et al.* [73] already pointed out that the local structure strongly depends on the sample preparation conditions, which is in line with the fact that 50:50 composition properties change drastically especially around the Ge–Te [75]. This illustrates how experimentally difficult it is to compare differently prepared glasses with each other. Caravati and coworkers showed via DFT simulations the coexistence of tetrahedral- and octahedral-like sites for Ge atoms in GST [20] and later in GeTe [23].

Our study allows a detailed look at the bond nature and reveals mostly threefold coordination. As this coordination might still arise from defective tetrahedra, we analyzed our structures grouped by conductivity to determine the bond-angle distribution irrespective of the number of bonds. Also, single atoms may have a mix of both octahedral and tetrahedral bond angles [cf. Fig. 2(f)]. We find an approximate normal distribution centered around about 95° but no clear bimodal distribution (see Supplemental Material [58]). Fitting the spectrum with two Gaussians, we get a ratio of roughly 2:1 octahedral to tetrahedral coordination, with no significant trend in terms of optical conductivity. Thus we conclude that there is no change in the ratio between octahedral and tetrahedral coordination upon relaxation in either direction.

Relaxation vs crystallization. Lee *et al.* [76–78] observed experimentally that the mid-range order in the phase-change material AIST (Ag/In-incorporated Sb_2Te) increases upon annealing below the crystallization temperature (thus upon relaxation). They conclude that it is the formation of subcritical crystalline nuclei that increase the mid-range order and speed up the crystallization process. This is in line with our finding of an increased number of Ge[3+1] and Te[3+1] coordination, which is the crystalline building block.

To evaluate whether those bond configurations also cluster upon annealing to realize mid-range order and nucleation sites, we analyzed our structures for correlated Ge[3+1] coordination, i.e., two Ge[3+1] centers being close together. There is a clear increase ($r = -0.57$) of correlated Ge[3+1] sites with conductivity. However, normalized to the overall increase of the Ge[3+1] centers, this correlation vanishes ($r = -0.16$). Hence, while upon relaxation more Ge[3+1] centers form, their ordering/clustering is not enhanced. Often, the structure of PCM has been analyzed in terms of rings and in particular of ABAB squares as proposed by Akola and coworkers [19]. We found that forming of Ge[3+1] upon

relaxation consumes rings made of Ge-Te pairs. Interestingly, the rings that are more consumed are those distorted from 90° , as illustrated in Fig. S3 in the Supplemental Material [58].

This seems to be the main difference between relaxation towards the ideal glass and crystallization. During relaxation, distorted rings and misaligned cubes are consumed, a structure with unordered Ge[3+1] is approached with both octahedral and tetrahedral bond angles in a 2:1 ratio. Upon crystallization, the structure orders, those Ge[3+1] sites form ABAB squares and then correctly oriented cubes by removing the tetrahedral bond angles [74,79,80]. Therefore, relaxation increases crystallization via nucleation, whereas crystal growth is slowed down because of the increased viscosity in relaxed structures [18,81].

This example demonstrates impressively how the inter-linked processes in phase-change materials result in a complex behavior that in the case of relaxation is a challenge for technology because of resistance drift, but that at the same time might be beneficial for data retention as crystal growth is inhibited even though crystal nucleation is enhanced.

V. CONCLUSIONS

In conclusion, we used a recently developed augmented Tersoff-based potential to generate GeTe structures via classical MD at the experimental conditions. For the first time, we used the replica-exchange scheme to model a-GeTe, which proved to be very effective in sampling the configurational space in amorphous materials, to generate additional structures representative of those obtained in the experiment after annealing that show an increase of resistance. We used DFT to compute the optical conductivity of each configuration to link structural modifications with changes of resistance. We found no change in the ratio between octahedral and tetrahedral coordination of Ge atoms upon relaxation. Our analysis shows that most of the defects in the gap are caused by groups of Ge atoms in which the coordination of at least one Ge atom differs from that of the crystalline phase: three bonds and one Wannier lone pair. We found that an increase in resistance is correlated with both a consumption of these defects in a-GeTe and accompanied by a slow evolution of the bond network towards structures having a first-neighbor topology more similar to that of the crystalline phase, which support our original findings [35] and recent results by Raty *et al.* [36] and Gabardi *et al.* [37]. Moreover, we showed that the increase of resistance is not produced by an increase of the band gap, which was instead reported by Raty *et al.* [36], but rather by a shift of the Fermi level towards the middle of the band gap. For a prototypical example we show the mechanisms and characterize the energy barrier along the reaction pathway at the DFT level. This study shows that an increase of rigidity of the bond network can prevent resistance drift via increasing the activation energy barriers for bond reorganization. Such increase of rigidity can be achieved by replacing a small fraction of Ge and Te atoms with atoms that can make stronger covalent bonds, e.g., by replacing part of Ge and Te with Si and Se atoms, respectively. Our findings are confirmed by Beneventi *et al.* [82] who reported a reduced drift by carbon-doped a-GeTe. During the revision of the manuscript

we found that a similar solution has also been proposed in Ref. [54].

ACKNOWLEDGMENTS

We would like to thank the PCM team at IBM Research–Zurich, in particular H. Pozidis and E. Eleftheriou, for their support of this work and C. Bolliger and I. Tavernelli for help with the preparation of the manuscript.

APPENDIX: AUTHOR CONTRIBUTIONS

A.C. proposed the approach to the modeling. F.Z. developed and implemented the approach and the original analysis with contributions from A.C. D.K. contributed with experimental insights and extended knowledge of the system. F.Z. and D.K. wrote the paper. All authors contributed to the scientific discussions, refining and clarifying the concepts presented by the manuscript, and read and discussed the paper.

-
- [1] S. Raoux, G. W. Burr, M. J. Breitwisch, C. T. Rettner, Y. C. Chen, R. M. Shelby, M. Salinga, D. Krebs, S. H. Chen, H. L. Lung, and C. H. Lam, *IBM J. Res. Dev.* **52**, 465 (2008).
- [2] G. W. Burr, M. J. Breitwisch, M. Franceschini, D. Garetto, K. Gopalakrishnan, B. Jackson, B. Kurdi, C. Lam, L. A. Lastras, A. Padilla, B. Rajendran, S. Raoux, and R. S. Shenoy, *J. Vac. Sci. Technol. B* **28**, 223 (2010).
- [3] M. Wuttig and N. Yamada, *Nat. Mater.* **6**, 824 (2007).
- [4] D. Lencer, M. Salinga, and M. Wuttig, *Adv. Mater.* **23**, 2030 (2011).
- [5] N. Papandreou, A. Pantazi, A. Sebastian, M. Breitwisch, C. Lam, H. Pozidis, and E. Eleftheriou, in *Proceedings of the 17th IEEE International Conference on Electronics, Circuits, and Systems (ICECS)* (IEEE, Piscataway, 2010), pp. 1017–1020.
- [6] N. Papandreou, H. Pozidis, T. Mittelholzer, G. Close, M. Breitwisch, C. Lam, and E. Eleftheriou, in *2011 3rd IEEE International Memory Workshop (IMW)* (IEEE, Piscataway, 2011), pp. 1–4.
- [7] D. Krebs, T. Bachmann, P. Jonnalagadda, L. Dellmann, and S. Raoux, *New J. Phys.* **16**, 043015 (2014).
- [8] A. Pirovano, A. L. Lacaíta, F. Pellizzer, S. A. Kostylev, A. Benvenuti, and R. Bez, *IEEE Trans. Electron Devices* **51**, 714 (2004).
- [9] M. Boniardi, A. Redaelli, A. Pirovano, I. Tortorelli, D. Ielmini, and F. Pellizzer, *J. Appl. Phys.* **105**, 084506 (2009).
- [10] D. Krebs, R. M. Schmidt, J. Klomfaß, J. Luckas, G. Bruns, C. Schlockermann, M. Salinga, R. Carius, and M. Wuttig, *J. Nron-Cryst. Solids* **358**, 2412 (2012).
- [11] P. Fantini, S. Brazzelli, E. Cazzini, and A. Mani, *Appl. Phys. Lett.* **100**, 013505 (2012).
- [12] J. Luckas, D. Krebs, M. Salinga, M. Wuttig, and C. Longeaud, *Physica Status Solidi C* **7**, 852 (2010); C. Longeaud, J. Luckas, D. Krebs, R. Carius, J. Klomfaß, and M. Wuttig, *J. Appl. Phys.* **112**, 113714 (2012); J. Luckas, D. Krebs, S. Grothe, J. Klomfaß, R. Carius, C. Longeaud, and M. Wuttig, *J. Mater. Res.* **28**, 1139 (2013).
- [13] G. Bruns, P. Merkelbach, C. Schlockermann, M. Salinga, M. Wuttig, T. D. Happ, J. B. Philipp, and M. Kund, *Appl. Phys. Lett.* **95**, 043108 (2009).
- [14] J. Baschnagel, K. Binder, and H. P. Wittmann, *J. Phys. Condens. Matter* **5**, 1597 (1993).
- [15] J. Buchholz, W. Paul, F. Varnik, and K. Binder, *J. Chem. Phys.* **117**, 7364 (2002).
- [16] S. L. Roux and P. Jund, *J. Phys. Condens. Matter* **19**, 196102 (2007).
- [17] F. Mallamace, C. Branca, C. Corsaro, N. Leone, J. Spooren, S.-H. Chen, and H. E. Stanley, *Proc. Nat. Acad. Sci. USA* **107**, 22457 (2010).
- [18] A. Sebastian, M. Le Gallo, and D. Krebs, *Nat. Commun.* **5**, 4314 (2014).
- [19] J. Akola and R. O. Jones, *Phys. Rev. B* **76**, 235201 (2007).
- [20] S. Caravati, M. Bernasconi, T. Kühne, M. Krack, and M. Parrinello, *Appl. Phys. Lett.* **91**, 171906 (2007).
- [21] J. Akola and R. O. Jones, *Phys. Rev. Lett.* **100**, 205502 (2008).
- [22] S. Caravati, M. Bernasconi, T. D. Khne, M. Krack, and M. Parrinello, *J. Phys. Condens. Matter* **21**, 255501 (2009).
- [23] R. Mazzarello, S. Caravati, S. Angioletti-Uberti, M. Bernasconi, and M. Parrinello, *Phys. Rev. Lett.* **104**, 085503 (2010).
- [24] J. Akola, J. Larrucea, and R. O. Jones, *Phys. Rev. B* **83**, 094113 (2011).
- [25] M. Krbal, A. V. Kolobov, P. Fons, J. Tominaga, S. R. Elliott, J. Hegedus, and T. Uruga, *Phys. Rev. B* **83**, 054203 (2011).
- [26] T. H. Lee and S. R. Elliott, *Phys. Rev. B* **84**, 094124 (2011).
- [27] B. Huang and J. Robertson, *Phys. Rev. B* **85**, 125305 (2012).
- [28] D. Loke, T. H. Lee, W. J. Wang, L. P. Shi, R. Zhao, Y. C. Yeo, T. C. Chong, and S. R. Elliott, *Science* **336**, 1566 (2012).
- [29] M. Krbal, A. Kolobov, P. Fons, K. Mitrofanov, Y. Tamenori, J. Hegedüs, S. Elliott, and J. Tominaga, *Appl. Phys. Lett.* **102**, 111904 (2013).
- [30] J. Skelton, D. Loke, T. Lee, and S. Elliott, *Phys. Status Solidi B* **250**, 968 (2013).
- [31] G. C. Sosso, G. Miceli, S. Caravati, F. Giberti, J. Behler, and M. Bernasconi, *The Journal of Physical Chemistry Letters* **4**, 4241 (2013).
- [32] F. Zipoli and A. Curioni, *New J. Phys.* **15**, 123006 (2013).
- [33] G. C. Sosso, G. Miceli, S. Caravati, J. Behler, and M. Bernasconi, *Phys. Rev. B* **85**, 174103 (2012).
- [34] J. Heyd, G. E. Scuseria, and M. Ernzerhof, *J. Chem. Phys.* **118**, 8207 (2003).
- [35] F. Zipoli and A. Curioni, EPCOS 2012 Proceedings 158 (2012) [<http://www.epcos.org/library/library2012.htm>]; EPCOS 2013 Proceedings 130 (2013) [<http://www.epcos.org/library/library2013.htm>].
- [36] J. Raty, W. Zhang, J. Luckas, C. Chen, R. Mazzarello, C. Bichara, and M. Wuttig, *Nat. Commun.* **6**, 7467 (2015).
- [37] S. Gabardi, S. Caravati, G. C. Sosso, J. Behler, and M. Bernasconi, *Phys. Rev. B* **92**, 054201 (2015).
- [38] Y. Sugita and Y. Okamoto, *Chem. Phys. Lett.* **314**, 141 (1999).
- [39] Y. Sugita and Y. Okamoto, *Chem. Phys. Lett.* **329**, 261 (2000).
- [40] P. A. Khomyakov, W. Andreoni, N. D. Afify, and A. Curioni, *Phys. Rev. Lett.* **107**, 255502 (2011).
- [41] A. Laio and M. Parrinello, *Proc. Nat. Acad. Sci. USA* **99**, 12562 (2002).
- [42] M. Iannuzzi, A. Laio, and M. Parrinello, *Phys. Rev. Lett.* **90**, 238302 (2003).

- [43] D. B. Dove, M. B. Heritage, K. L. Chopra, and S. K. Bahl, *Appl. Phys. Lett.* **16**, 138 (1970).
- [44] G. E. Ghezzi, J. Y. Raty, S. Maitrejean, A. Roule, E. Elkaim, and F. Hippert, *Appl. Phys. Lett.* **99**, 151906 (2011).
- [45] G. C. Sosso, J. Colombo, J. Behler, E. Del Gado, and M. Bernasconi, *J. Phys. Chem. B* **118**, 13621 (2014).
- [46] H. J. C. Berendsen, J. P. M. Postma, W. F. van Gunsteren, A. DiNola, and J. R. Haak, *J. Chem. Phys.* **81**, 3684 (1984).
- [47] N. Metropolis, A. W. Rosenbluth, M. N. Rosenbluth, A. H. Teller, and E. Teller, *J. Chem. Phys.* **21**, 1087 (1953).
- [48] J. P. Perdew, K. Burke, and M. Ernzerhof, *Phys. Rev. Lett.* **77**, 3865 (1996).
- [49] Computer code CPMD, IBM, Armonk, 1990–2015 and Max Planck Institut für Festkörperforschung, Stuttgart, Germany, 1997–2001.
- [50] S. Caravati, M. Bernasconi, and M. Parrinello, *J. Phys. Condens. Matter* **22**, 315801 (2010).
- [51] Y. Maeda and M. Wakagi, *Jpn. J. Appl. Phys.* **30**, 101 (1991).
- [52] H. Flores-Ruiz, M. Micoulaut, M.-V. Coulet, A. A. Piarristeguy, M. R. Johnson, G. J. Cuello, and A. Pradel, *Phys. Rev. B* **92**, 134205 (2015).
- [53] S. Goedecker, M. Teter, and J. Hutter, *Phys. Rev. B* **54**, 1703 (1996).
- [54] J.-Y. Raty, C. Otyjacques, R. Peköz, V. Lordi, and C. Bichara, *Amorphous Phase Change Materials: Structure, Stability and Relation with their Crystalline Phase* (Springer, New York, 2015).
- [55] N. Marzari and D. Vanderbilt, *Phys. Rev. B* **56**, 12847 (1997).
- [56] P. L. Silvestrelli, N. Marzari, D. Vanderbilt, and M. Parrinello, *Solid State Commun.* **107**, 7 (1998).
- [57] P. L. Silvestrelli and M. Parrinello, *Phys. Rev. Lett.* **82**, 3308 (1999).
- [58] See Supplemental Material at <http://link.aps.org/supplemental/10.1103/PhysRevB.93.115201> for details on the CPMD simulations and on the choice of the reaction coordinated for the metadynamics simulation.
- [59] G. Henkelman, B. P. Uberuaga, and H. Jónsson, *J. Chem. Phys.* **113**, 9901 (2000).
- [60] W. H. Zachariasen, *J. Am. Chem. Soc.* **54**, 3841 (1932).
- [61] M. H. Cohen, H. Fritzsche, and S. R. Ovshinsky, *Phys. Rev. Lett.* **22**, 1065 (1969).
- [62] N. F. Mott and R. A. Street, *Philos. Mag.* **36**, 33 (1977).
- [63] N. F. Mott and E. A. Davis, *Electronic Processes in Non-Crystalline Materials*, 2nd Ed. (Oxford University Press, Oxford, 1979).
- [64] A. V. Kolobov, P. Fons, and J. Tominaga, *Phys. Rev. B* **87**, 155204 (2013).
- [65] A. V. Kolobov, P. Fons, and J. Tominaga, *Sci. Rep.* **5**, 13698 (2015).
- [66] V. L. Deringer, W. Zhang, M. Lumeij, S. Maintz, M. Wuttig, R. Mazzarello, and R. Dronskowski, *Angewandte Chemie International Edition* **53**, 10817 (2014).
- [67] M. Gibbs, J. Evetts, and J. Leake, *J. Mater. Sci.* **18**, 278 (1983).
- [68] A. Knoll, D. Wiesmann, B. Gotsmann, and U. Duerig, *Phys. Rev. Lett.* **102**, 117801 (2009).
- [69] T. Egami, *J. Mater. Sci.* **13**, 2587 (1978).
- [70] M. Kastner, D. Adler, and H. Fritzsche, *Phys. Rev. Lett.* **37**, 1504 (1976).
- [71] E. O'Reilly, J. Robertson, and M. Kelly, *Solid State Commun.* **38**, 565 (1981).
- [72] T. Takahashi, H. Sakurai, and T. Sagawa, *Solid State Commun.* **44**, 723 (1982).
- [73] S. Hosokawa, Y. Hari, T. Kouchi, I. Ono, H. Sato, M. Taniguchi, A. Hiraya, Y. Takata, N. Kosugi, and M. Watanabe, *J. Phys. Condens. Matter* **10**, 1931 (1998).
- [74] K. V. Mitrofanov, A. V. Kolobov, P. Fons, X. Wang, J. Tominaga, Y. Tamenori, T. Uruga, N. Ciocchini, and D. Ielmini, *J. Appl. Phys.* **115**, 173501 (2014).
- [75] M. Chen, K. A. Rubin, and R. W. Barton, *Appl. Phys. Lett.* **49**, 502 (1986).
- [76] B.-S. Lee, G. W. Burr, R. M. Shelby, S. Raoux, C. T. Rettner, S. N. Bogle, K. Darmawikarta, S. G. Bishop, and J. R. Abelson, *Science* **326**, 980 (2009).
- [77] B.-S. Lee, K. Darmawikarta, S. Raoux, Y.-H. Shih, Y. Zhu, S. G. Bishop, and J. R. Abelson, *Appl. Phys. Lett.* **104**, 071907 (2014).
- [78] B.-S. Lee, R. M. Shelby, S. Raoux, C. T. Rettner, G. W. Burr, S. N. Bogle, K. Darmawikarta, S. G. Bishop, and J. R. Abelson, *J. Appl. Phys.* **115**, 063506 (2014).
- [79] K. Shportko, S. Kremers, M. Woda, D. Lencer, J. Robertson, and M. Wuttig, *Nat. Mater.* **7**, 653 (2008).
- [80] B. Huang and J. Robertson, *Phys. Rev. B* **81**, 081204 (2010).
- [81] M. Salinga, E. Carria, A. Kaldenbach, M. Bornhft, J. Benke, J. Mayer, and M. Wuttig, *Nat. Commun.* **4**, 2371 (2013).
- [82] G. B. Beneventi, L. Perniola, V. Sousa, E. Gourvest, S. Maitrejean, J. Bastien, A. Bastard, B. Hyot, A. Fargeix, C. Jahan, J. F. Nodin, A. Persico, A. Fantini, D. Blachier, S. Toffoli, A. Loubriat, A. Roule, S. Lhostis, H. Feldis, G. Reibold, T. Billon, B. De Salvo, L. Larcher, P. Pavan, D. Bensahel, P. Mazoyer, R. Annunziata, P. Zuliani, and F. Boulanger, *Solid-State Electron.* **65-66**, 197 (2011).